

CERN-TH/2002-111
IPPP/02/28
DCPT/02/56
UCRHEP-T340
June 2002
Revised August 2002

THE τ -POLARISATION TEST FOR THE $H/A \rightarrow \tau^+\tau^-$ SIGNAL AT THE LHC

S. Moretti^{a,1} and D.P. Roy^{b,2}

^a *CERN Theory Division, CH-1211 Geneva 23, Switzerland*

and

Institute for Particle Physics Phenomenology, University of Durham, Durham DH1 3LE, UK

^b *Tata Institute of Fundamental Research, Mumbai, 400 005, India*

and

Physics Department, University of California, Riverside, CA 92521, U.S.A.

ABSTRACT

The correlation between the two τ -polarisations is predicted to be opposite (+ - / - +) for the $H/A \rightarrow \tau^+\tau^-$ signal, while it corresponds to the same sign combinations for the Drell-Yan (+ + / - -) and $t\bar{t}$ (- -) backgrounds. We show that this correlation can serve as a distinctive test to confirm the presence of the MSSM Higgs bosons H and A in their hadronic $\tau^+\tau^-$ decay channels at the LHC.

¹stefano.moretti@cern.ch

²dproy@theory.tifr.res.in

The Minimal Supersymmetric Standard Model (MSSM) contains two Higgs doublets [1]. The ratio of their vacuum expectation values is denoted by $\tan\beta$, which is required to be larger than 2 by the LEP data [2, 3]. The two complex scalar doublets correspond to eight independent fields, three of which are absorbed by the W^\pm and Z bosons. Thus we are left with five physical states: two neutral scalars h and H , a neutral pseudoscalar A , along with a pair of charged Higgs bosons H^\pm . For large M_A values ($\gg M_Z$), the two heavy neutral Higgs bosons, H and A , have similar masses and couplings. On the one hand, the H/A boson couplings to the top quark are suppressed by a factor of $\cot\beta$ relative to that of the Standard Model (SM) Higgs boson, while they both decouple from the W^\pm and Z bosons. On the other hand, their couplings to the bottom quark are enhanced by a factor of $\tan\beta$ relative to that of the SM Higgs boson. Thus one expects a large H/A production signal at the Large Hadron Collider (LHC) over the large $\tan\beta$ region via the $b\bar{b} \rightarrow H/A$ ‘fusion’ mechanism. Moreover the H/A couplings to the τ lepton are also enhanced by a factor of $\tan\beta$ over this region.

Therefore the $H/A \rightarrow \tau^+\tau^-$ decay channel provides the most promising signature for the two heavier neutral Higgs bosons of the MSSM at the LHC. Simulation studies have shown this decay channel to be viable over a large part of the parameter space of the model [2, 3]. Moreover, a systematic study of this process in both the leptonic and hadronic decay channels of the τ ’s [4, 5] shows that the latter has two advantages, i.e., a larger branching ratio (BR) and a larger visible fraction of the τ -energy/momentum. This implies that one can reconstruct the $\tau^+\tau^-$ invariant mass most precisely via

$$\tau^+\tau^- \rightarrow h^+h^-\nu\nu \quad (1)$$

(hereafter, h^\pm represents a generic charged hadron) [4]. This channel is particularly useful for relatively large values of the two MSSM parameters defining the Higgs sector of the MSSM at tree level, i.e., $M_A \gtrsim 200$ GeV and $\tan\beta \gtrsim 15$. This area is precisely where the two Higgs states H and A are degenerate in their masses and couplings.

In this note, we shall analyse a distinctive feature of the $H/A \rightarrow \tau^+\tau^-$ signal that has not received much attention so far, i.e., the correlation between the τ -polarisations. It simply follows from angular momentum conservation that the $\tau^+\tau^-$ pairs emerging from the H/A decays have opposite polarisations, i.e.,

$$H/A \rightarrow \tau^+\tau^- X, \quad P_{\tau^+}(P_{\tau^-}) = \pm 1(\mp 1). \quad (2)$$

In contrast, the main irreducible backgrounds from Drell-Yan (DY) and top-antitop processes predict the same polarisation for the $\tau^+\tau^-$ pair, i.e.,

$$\gamma^*/Z \rightarrow \tau^+\tau^- X, \quad P_{\tau^+}(P_{\tau^-}) = \pm 1(\pm 1), \quad (3)$$

$$t\bar{t} \rightarrow b\bar{b}W^+W^- \rightarrow \tau^+\tau^- X, \quad P_{\tau^+}(P_{\tau^-}) = -1(-1). \quad (4)$$

The distinctive τ -polarisations for the above signal and background processes were first discussed in Ref. [6], along with the analogous distinction between the charged Higgs signal and the W^\pm background, i.e.,

$$H^\pm \rightarrow \tau^\pm\nu, \quad P_{\tau^\pm} = +1; \quad W^\pm \rightarrow \tau^\pm\nu, \quad P_{\tau^\pm} = -1. \quad (5)$$

The possibility of measuring the predicted τ -polarisations via their hadronic decays was also discussed there. Meanwhile, quantitative Monte Carlo (MC) studies of the charged Higgs boson signal at the LHC have shown the polarisation distinction in (5) to be a very powerful tool in separating the H^\pm and W^\pm contributions in the hadronic τ -decay channels [7, 8]. To the best of our knowledge, however, there has been no such quantitative study for the neutral Higgs signal in (2). Of course, one can see from Eqs. (2)–(4) that the polarisation distinction for the neutral Higgs signal is more subtle than the charged Higgs case, Eq. (5). In particular, the average τ -polarisation for the $H/A \rightarrow \tau^+\tau^-$ signal is 0. The same is also true for the DY background in (3), since the vector coupling of γ and the dominantly axial coupling of Z imply that the polarisation combinations $++$ and $--$ occur with almost equal probability. Nonetheless, we shall see below that the correlation between the τ -polarisations can be effectively used to distinguish the signal from the background in the hadronic $\tau^+\tau^-$ channel.

Our results are based on a parton level MC simulation of the H/A signal in (2) as well as the γ^* , Z and $t\bar{t}$ background processes in (3) and (4). The dominant signal process in the large $\tan\beta$ ($\gtrsim 15$) region of interest can be emulated via associate production with b -quarks [9]:

$$gg, q\bar{q} \rightarrow b\bar{b}H/A. \quad (6)$$

The cross sections for process (6) have been calculated by several groups [10]. While these references do not give compact formulae, the latter are very similar to those for $gg, q\bar{q} \rightarrow t\bar{t}H^-$, described in detail in Ref. [11], which have been used again here, after rearranging the Higgs-to-fermion couplings appropriately. The formulae for the H/A decay rates are taken from Ref. [12] (see also [13]). The DY and top-antitop background processes are computed using MadGraph [14]. The phase space integrations have been done numerically with the help of VEGAS [15]. We have used the parton distribution functions MRS99(COR01) [16], evaluated at the scale $\mu = M_H(M_A)$ for the signal and $\mu = \sqrt{\hat{s}}/2(2m_t)$ for the γ^* , $Z(t\bar{t})$ backgrounds. (The results for these two processes are however insensitive to the precise value of these scales.) The ‘running’ expression of the b -quark mass was used for the Yukawa coupling of the signal process.

To emulate detector resolution, we have applied Gaussian smearing on the transverse momentum of each parton jet (including the τ -jets) with

$$(\sigma(p_T)/p_T)^2 = (0.6/\sqrt{p_T})^2 + (0.04)^2 \quad (7)$$

in GeV units. The missing transverse momentum, p_T^{miss} , is reconstructed from the vector sum of the jet p_T ’s after resolution smearing. Following Ref. [4], we have imposed the following selection cuts on the two τ -jets and the accompanying missing transverse momentum:

$$\begin{aligned} \Delta R(\text{jet} - \text{jet}) &> 0.4, & p_T(\tau\text{-jets}) &> 60 \text{ GeV}, & |\eta(\tau\text{-jets})| &< 2.5, \\ \Delta\phi(\tau\text{-jets}) &< 175^\circ, & p_T^{\text{miss}} &> 40 \text{ GeV}. \end{aligned} \quad (8)$$

As in Ref. [4], we shall concentrate on the 1-prong hadronic decay channels of τ ’s, which are best suited for distinguishing τ -jets from the QCD background. With the above cuts, the QCD background has been estimated to be relatively small compared to the DY and top-antitop ones [4]. While the DY background could be suppressed by b -tagging, it would also reduce the signal size significantly. Therefore, we do not require any b -tagging, just like Ref. [4].

The 1-prong hadronic decay channel of τ 's accounts for 80% of its hadronic decay width and 50% of the total width. The main contributors to the 1-prong hadronic decay are

$$\tau^\pm \rightarrow \pi^\pm \nu(12\%), \quad \rho^\pm \nu(26\%), \quad a_1^\pm \nu(8\%), \quad (9)$$

where the BRs for π and ρ include the small K and K^* contributions, respectively, which have identical polarisation effects [17]. The centre-of-mass (CM) angular distribution of τ -decays into π or a vector meson $v(= \rho, a_1)$ is simply given in terms of its polarisation as

$$\frac{1}{\Gamma_\pi} \frac{d\Gamma_\pi}{d\cos\theta} = \frac{1}{2}(1 + P_\tau \cos\theta), \quad (10)$$

$$\frac{1}{\Gamma_v} \frac{d\Gamma_{v\ L,T}}{d\cos\theta} = \frac{\frac{1}{2}m_\tau^2, m_v^2}{m_\tau^2 + 2m_v^2}(1 \pm P_\tau \cos\theta), \quad (11)$$

where L, T denote the longitudinal and transverse polarisation states of the vector meson. The fraction x of τ -momentum in the laboratory frame carried by its decay hadron is related to the polar angle θ via

$$x = \frac{1}{2}(1 + \cos\theta) + \frac{m_{\pi,v}^2}{2m_\tau^2}(1 - \cos\theta), \quad (12)$$

in the collinear approximation. Thus the visible momentum of τ , which defines the momentum of the τ -jet, is

$$p_{\tau\text{-jet}} \equiv p_{\text{hadron}} = xp_\tau. \quad (13)$$

We see from Eqs. (10)–(13) that $P_\tau = +1$ gives a harder τ -jet than $P_\tau = -1$.

We can also see from Eqs. (10)–(13) that the hard τ -jet is dominated by the π and the longitudinal vector meson (ρ_L, a_{1L}) contributions for $P_\tau = +1$, while it is dominated by the transverse ρ and a_1 (ρ_T, a_{1T}) contributions for $P_\tau = -1$. The two sets can be distinguished by exploiting the fact that the transverse ρ and a_1 decays favour even sharing of momentum between the decay pions, while the longitudinal ρ and a_1 decays favour uneven sharing, where the charged pion carries very little or most of the meson momentum. One can measure the fraction of the visible τ -jet momentum, carried by the charged pion,

$$R = p_{\pi^\pm}/p_{\tau\text{-jet}}, \quad (14)$$

by combining the charged prong momentum measurement in the tracker with the calorimetric energy deposit of the τ -jet. Then the hard τ -jet is predicted to show peaks at $R \simeq 0$ and 1 for $P_\tau = +1$ and at $R \simeq 0.4$ for $P_\tau = -1$ [6, 7]. Note that the $\tau^\pm \rightarrow \pi^\pm \nu$ contribution adds substantially to the $R \simeq 1$ peak for $P_\tau = +1$, while it is suppressed for $P_\tau = -1$. One can easily derive the above results quantitatively for $\rho_{L,T}$ decays; but one has to assume a dynamical model for the a_1 decay for a quantitative result.

We shall adopt the model of Ref. [18], based on a conserved axial-vector current approximation, which describes the $a_1 \rightarrow 3\pi$ decay data very well. A detailed account of the ρ and a_1 decay formalisms including finite width effects can be found in Refs. [6, 7]. A simple FORTRAN code for 1-prong hadronic decays of polarised τ -leptons based on these formalisms can be obtained from one of the authors.

Before discussing the results, let us briefly describe the reconstruction of the $\tau^+\tau^-$ invariant mass. The $\Delta\phi$ cut of Eq. (8) ensures that the transverse momenta of the two τ -jets, p_{T1} and p_{T2} , are not in the back-to-back configuration. In this case, one can resolve the p_T^{miss} along their directions and add it to p_{T1} and p_{T2} . Scaling up the respective sums by the ratios p_1/p_{T1} and p_2/p_{T2} gives the reconstructed momenta of the $\tau^+\tau^-$ pair. The resulting $\tau^+\tau^-$ invariant mass represents the H/A mass for the signal process (2) and the γ^*/Z mass for the DY background (3); but it does not represent any physical quantity for the $t\bar{t}$ background (4), since the latter contains additional sources of missing momentum.

The production cross sections of the H and A bosons are practically identical in the large $\tan\beta$ region of our interest. As an illustration, we have calculated the signal cross sections for

$$\tan\beta = 15 \quad \text{and} \quad M_A = M_H = 200(300) \text{ GeV}, \quad (15)$$

which is at the edge of the discovery limit for this channel [4, 8].

Fig. 1 shows the signal and background cross sections against the reconstructed $\tau^+\tau^-$ invariant mass. We see that a $M_{\tau\tau}$ cut of 150–300(200–400) GeV will suppress the DY and top-antitop backgrounds without any appreciable loss of the 200(300) GeV H/A signal. Therefore, we shall impose these invariant mass cuts in the remainder of our analysis. Let us first consider the $M_{H,A} = 200$ GeV case. The signal and background cross sections for this case are shown on the top row of Tab. 1. They are seen to be of similar size. With an expected luminosity of 300 fb^{-1} at the LHC, they correspond to about 1000 signal events over a background of roughly similar size. This constitutes a comfortably large S/\sqrt{B} ratio.

$M_{H,A}$ (GeV)	bbA	bbH	γ^*, Z	$t\bar{t}$
200	1.58	1.57	3.03	0.73
300	1.88	1.86	4.14	0.60
$\tan\beta = 15$				

Table 1: Cross sections in femtobarns for Higgs signals and backgrounds in the $\tau^+\tau^-X$ channel, after the selection cuts of Eq. (8). In addition, we have imposed a $M_{\tau\tau}$ cut of 150–300 GeV for $M_{H,A} = 200$ GeV and 200–400 GeV for $M_{H,A} = 300$ GeV. We have also imposed a stronger p_T cut of 100 GeV on the harder τ -jet in the latter case.

Fig. 2 shows the three-dimensional (3-D) plots of the 200 GeV H/A signals along with the DY and $t\bar{t}$ backgrounds against R_1, R_2 , the fractional τ -jet momenta carried by the charged prongs. The subscript 1(2) refers to the harder(softer) of the two τ -jets. There are several points worth noting in this figure. The τ -identification will require a minimum hardness for the charged prongs, presumably R_1 and $R_2 > 0.2$. Thus the $R_{1,2} < 0.2$ contributions from ρ_L and a_{1L} will not be relevant for the practical analysis. However, the peaks at $R_{1,2} \simeq 0.4$ and $R_{1,2} \simeq 1$, coming from the ρ_T, a_{1T} and ρ_L, π respectively, can be used to distinguish between the $P_\tau = -1$ and $+1$ contributions. In particular, the $t\bar{t}$ background, corresponding to the polarisation combination $--$, is crowded around $R_{1,2} \simeq 0.4$. In contrast, the signal is peaked

at R_1 or $R_2 > 0.8$, as expected for the polarisation combination $+-$. The same is seen to be true for the DY background, because the $p_T > 60$ GeV cut on the τ -jets has suppressed the $--$ contribution with respect to the $++$ combination. Thus requiring at least one of the two τ -jets to contain a very hard charged prong, carrying $> 80\%$ of its visible momentum, will suppress the $t\bar{t}$ background effectively without any significant loss to the signal or the DY background. Moreover, we expect this requirement to suppress the QCD background to an even greater extent than the $t\bar{t}$ background, because its R distributions are softer than those of the latter [4]. Therefore, we strongly advocate an asymmetric cut, requiring at least one of the R_1 and R_2 to be > 0.8 , for effective suppression of the $t\bar{t}$ and QCD backgrounds (including $W + \text{jets}$). Then the signal can be distinguished from the remaining DY background by looking at the asymmetric region: $R_1 > 0.8$ and $R_2 = 0.2 - 0.8$ and vice versa. The signal(DY background) has a peak(dip) in this region as expected from the polarisation correlation $+-(++)$. We have estimated 55% of the signal events to come from this asymmetric region as against 43% for the DY background. Thus excluding the symmetric region will improve the S/B ratio, but not the S/\sqrt{B} . On the other hand, the distribution of events between the symmetric and asymmetric regions can be used to distinguish the signal from the DY background. From an event sample of ~ 1000 one expects 550 to populate the above asymmetric region for the signal ($+-$) as against 430 for the background ($++$), which constitutes a $\gtrsim 5\sigma$ excess.

For higher H/A masses it may be more advantageous to use asymmetric p_T cuts on the two τ -jets. Fig. 3 shows the 300 GeV H/A signal along with the corresponding DY and $t\bar{t}$ backgrounds against the p_T of the harder τ -jet. It shows that increasing the p_{T1} cut to 100 GeV (while keeping the p_{T2} cut at 60 GeV) will suppress the $t\bar{t}$ background to a much higher degree than the signal, as expected from their polarisation combinations, $--$ and $-+$, respectively. The DY background is also suppressed to a somewhat larger extent than the signal, though the difference is rather modest (7–8%) in this case. The $p_{T2} > 60$ GeV cut is already suppressing the $--$ contribution with respect to the $++$ combination even for $M_{\tau\tau} \simeq 300$ GeV. We expect this difference to increase for higher H/A masses. We also expect the higher p_{T1} cut to be very effective in suppressing the QCD background (again, including $W+\text{jets}$). Tab. 1 shows the 300 GeV H/A signal cross sections along with the DY and $t\bar{t}$ backgrounds for this asymmetric cut (i.e., $p_{T1} > 100$ GeV, $p_{T2} > 60$ GeV). Their sizes are similar to the 200 GeV signal and background cross sections with symmetric p_T cuts. We expect the asymmetric p_T cuts to be advantageous in probing the region $M_{A/H} \gtrsim 300$ GeV.

Fig. 4 shows the 3-D plots of the 300 GeV H/A signal along with the DY and $t\bar{t}$ backgrounds against R_1 and R_2 for the asymmetric p_T cuts mentioned above. Most of the observations made for Fig. 2 apply to this case as well. In particular, one sees a peak(dip) for the signal(DY background) at $R_1 > 0.8$ and $R_2 = 0.2 - 0.8$, as expected from the polarisation correlation $+-(++)$. Note, however, that there is no clear peak for the signal in the complementary region, $R_2 > 0.8$ and $R_1 = 0.2 - 0.8$. This is because in this case the $p_{T2} > 60$ GeV cut is not hard enough to suppress the pion peak (at $R_2 = 1$) for $P_{\tau_2} = -1$. Consequently, the accompanying τ_1 has a significant component of $P_{\tau_1} = +1$. Thus for higher H/A masses one should look for the signal peak in the $R_1 > 0.8$ and $R_2 = 0.2 - 0.8$ region only. Nonetheless the difference is very significant in this case. About 30% of the 300 GeV H/A signal events populate this asymmetric region against 20% of the DY background events. This constitutes a

7σ excess for an event sample of ~ 1000 , which can be used as a confirmatory test of the H/A signal.

Finally, notice that the percentages of the signal and background events populating the asymmetric region are independent of the normalisation uncertainties of the various processes, since they depend entirely on the polarisations of the latter. The former mainly stem from higher order corrections due to QCD. While these are relatively well under control for the two backgrounds considered here, they can be very large for the signal (see [19] for an up-to-date discussion).

In summary, we have found that the correlation between the τ -polarisations are likely to play a very useful role in distinguishing the H/A signal from the backgrounds in the hadronic $\tau^+\tau^-$ channel at LHC. In view of the importance of this channel in the MSSM Higgs search programme at the LHC, it is imperative that this analysis is followed up with a more rigorous MC simulation, incorporating jet hadronisation and detector acceptance effects. We have currently undertaken such a simulation study [20] using the HERWIG event generator [21, 22] interfaced with the TAUOLA package [23, 24] for polarised τ -decays.

We gratefully acknowledge discussions with P. Aurenche, D. Denegri., R. Kinnunen and A. Nikitenko.

References

- [1] J.F. Gunion, H.E. Haber, G.L. Kane and S. Dawson, “The Higgs Hunter Guide” (Addison-Wesley, Reading MA, 1990), Erratum, preprint SCIPP-92-58, February 1993, hep-ph/9302272.
- [2] A. Djouadi et al., Higgs Working Group Summary Report of the 1st Les Houches Workshop on Physics at TeV Colliders, France (1999), hep-ph/0002258.
- [3] D. Cavalli et al., Higgs Working Group Summary Report of the 2nd Les Houches Workshop of Physics at TeV Colliders, France (2001), hep-ph/0203056.
- [4] R. Kinnunen and D. Denegri, CMS Note-199/037, hep-ph/9907291.
- [5] J. Thomas, ATLAS Note (in preparation).
- [6] B.K. Bullock, K. Hagiwara and A.D. Martin, Phys. Rev. Lett. 67 (1991) 3055; Nucl. Phys. B395 (1993) 494.
- [7] S. Raychaudhuri and D.P. Roy, Phys. Rev. D52 (1995) 1556; Phys. Rev. D53 (1996) 4902; D.P. Roy, Phys. Lett. B277 (1992) 183; Phys. Lett. B459 (1999) 607.
- [8] K.A. Assamagan, Y. Coadou and A. Deandrea, hep-ph/0203121; D. Denegri et al., hep-ph/0112045.
- [9] D.A. Dicus, T. Stelzer, Z. Sullivan and S.S.D. Willenbrock, Phys. Rev. D59 (1999) 094016.

- [10] Z. Kunszt, Nucl. Phys. B247 (1984) 339; J.F. Gunion, Phys. Lett. B253 (1991) 269; W.J. Marciano and F.E. Paige, Phys. Rev. Lett. 66 (1991) 2433; D.A. Dicus and S.S.D. Willenbrock, Phys. Rev. D39 (1989) 751.
- [11] D.J. Miller, S. Moretti, D.P. Roy and W.J. Stirling, Phys. Rev. D61 (2000) 055011; S. Moretti and D.P. Roy, Phys. Lett. B470 (1999) 209.
- [12] S. Moretti and W.J. Stirling, Phys. Lett. B347 (1995) 291, Erratum-ibidem B366 (1996) 451.
- [13] A. Djouadi, J. Kalinowski and P.M. Zerwas, Z. Phys. C70 4(1996) 35.
- [14] T. Stelzer and W.F. Long, Comput. Phys. Comm. 81, (1994) 357.
- [15] G.P. Lepage, Jour. Comp. Phys. 27 (1978) 192.
- [16] A.D. Martin, R.G. Roberts, W.J. Stirling and R.S. Thorne, Eur. Phys. J. C14 (2000) 133.
- [17] Particle Data Group, Eur. Phys. J. C15 (2002).
- [18] J.H. Kühn and A. Santamaria, Z. Phys. C48 (1990) 445.
- [19] See, e.g.: S. Balatenychev et al., in Ref. [3].
- [20] F. Moortgat, S. Moretti and D.P. Roy, in preparation.
- [21] G. Marchesini, B.R. Webber, G. Abbiendi, I.G. Knowles, M.H. Seymour and L. Stanco, Comput. Phys. Commun. 67 (1992) 465; G. Corcella, I.G. Knowles, G. Marchesini, S. Moretti, K. Odagiri, P. Richardson, M.H. Seymour and B.R. Webber, hep-ph/9912396; JHEP 0101 (2001) 010; hep-ph/0107071; hep-ph/0201201.
- [22] S. Moretti, K. Odagiri, P. Richardson, M.H. Seymour and B.R. Webber, JHEP 0204 (2002) 028; S. Moretti, hep-ph/0205105.
- [23] S. Jadach, Z. Was, R. Decker and J.H. Kuhn, Comput. Phys. Commun. 76 (1993) 361; M. Jezabek, Z. Was, S. Jadach and J.H. Kuhn, Comput. Phys. Commun. 70 (1992) 69; S. Jadach, J.H. Kuhn and Z. Was, Comput. Phys. Commun. 64 (1990) 275.
- [24] M. Worek, Acta Phys. Polon. B32 (2001) 3803.

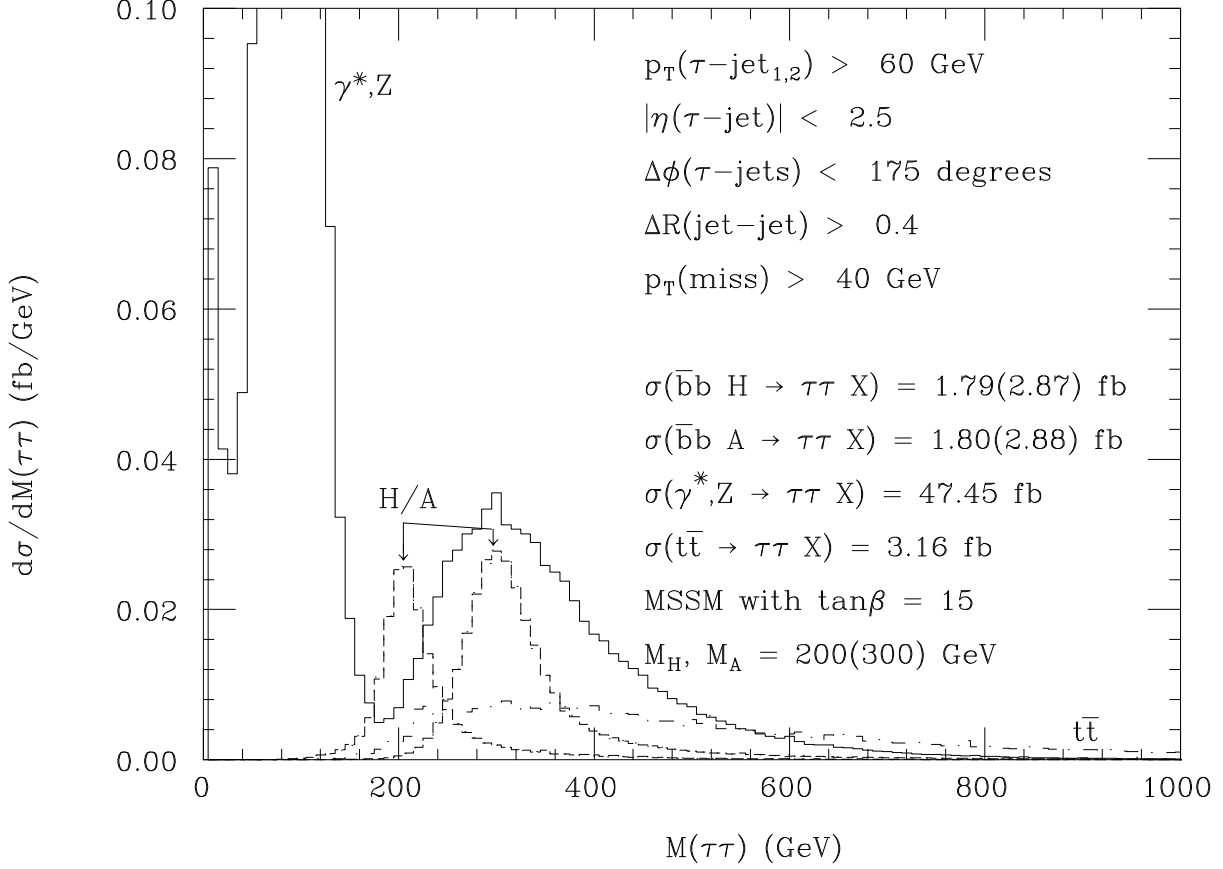
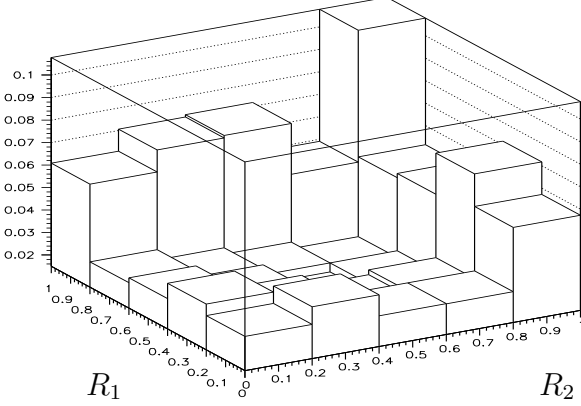


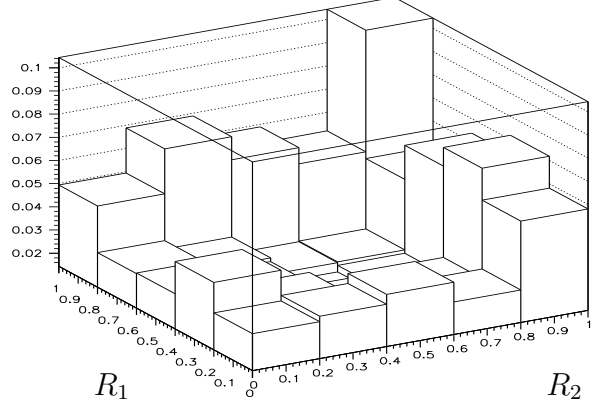
Figure 1: Singly differential distributions in the reconstructed $\tau^+\tau^-$ invariant mass in 1-prong hadronic decays, for the Higgs signals (dashed and dotted lines for H and A , respectively, coinciding visually) and backgrounds (solid and dot-dashed lines for DY and top-antitop, respectively) in the $\tau^+\tau^-X$ channel, after the following selection cuts (at parton level): $p_T(\tau - \text{jet}_{1[2]}) > 60[60] \text{ GeV}$ (1[2] refers to the most[least] energetic), $|\eta(\tau - \text{jet})| < 2.5$, $\Delta\Phi(\tau - \text{jets}) < 175^\circ$, $\Delta R(\text{jet-jet}) > 0.4$ and $p_T^{\text{miss}} > 40 \text{ GeV}$. Normalisations are to the total cross sections at $\sqrt{s} = 14 \text{ TeV}$ (for $M_A = M_H = 200(300) \text{ GeV}$ and $\tan\beta = 15$, in the case of the signal). Bins are 10 GeV wide.

$$\boxed{d^2\sigma/dR_1/dR_2/\sigma}$$

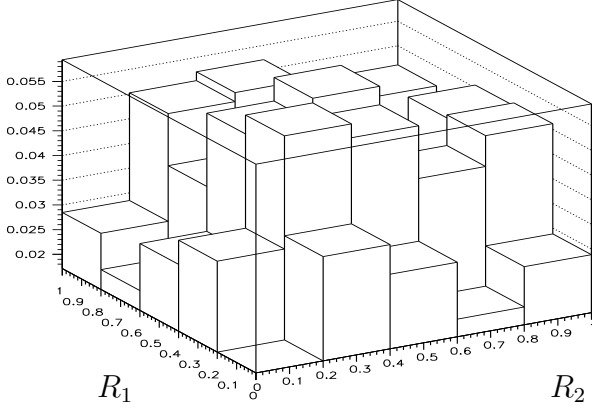
$b\bar{b}A \rightarrow \tau^+\tau^-X$ ($M_A = 200$ GeV)



$b\bar{b}H \rightarrow \tau^+\tau^-X$ ($M_H = 200$ GeV)



$t\bar{t} \rightarrow \tau^+\tau^-X$



$\gamma^*, Z \rightarrow \tau^+\tau^-X$

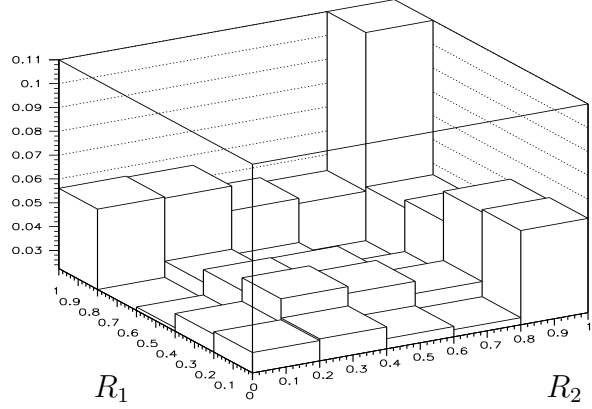


Figure 2: Doubly differential distributions in the energy fractions $R_i = p_i^{\pi^\pm} / p_i^{\tau\text{-jet}}$, where $p_i^{\pi^\pm}$ is the charged pion momentum and $p_i^{\tau\text{-jet}}$ that of the visible τ -jet, i.e, the momentum carried away by the mesons π^\pm, ρ^\pm and a_1^\pm in 1-prong decays, for Higgs signals and backgrounds in the $\tau^+\tau^-X$ channel (with $p_1 > p_2$), after the following selection cuts (at parton level): $p_T(\tau\text{-jet}_{1[2]}) > 60[60]$ GeV (1[2] refers to the most[least] energetic), $|\eta(\tau\text{-jet})| < 2.5$, $\Delta\Phi(\tau\text{-jets}) < 175^\circ$, $\Delta R(\text{jet-jet}) > 0.4$, $p_T^{\text{miss}} > 40$ GeV and $150 \text{ GeV} < M_{\tau\tau} < 300$ GeV. Normalisations are to unity at $\sqrt{s} = 14$ TeV (for $M_A = M_H = 200$ GeV in the case of the signal). Bins are 0.2 units wide.

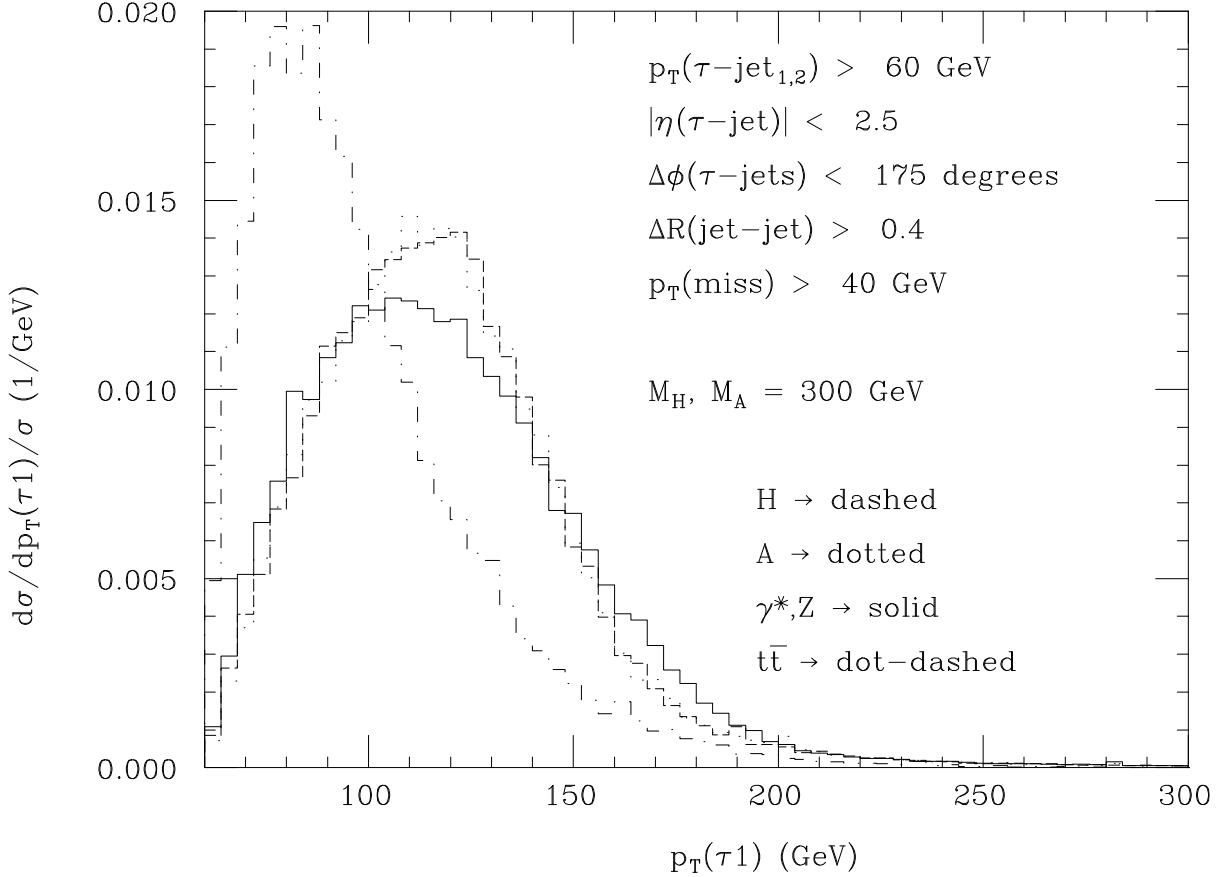
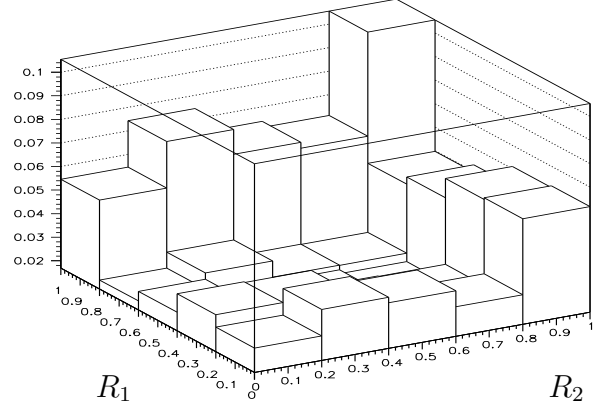
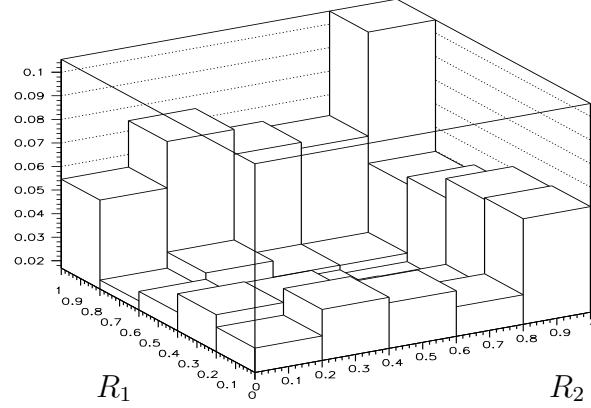


Figure 3: Singly differential distributions in the transverse momentum of the most energetic τ -jet in 1-prong decays, for Higgs signals and backgrounds in the $\tau^+\tau^-X$ channel, after the following selection cuts (at parton level): $p_T(\tau - \text{jet}_{1[2]}) > 60[60]$ GeV (1[2] refers to the most[least] energetic), $|\eta(\tau - \text{jet})| < 2.5$, $\Delta\Phi(\tau - \text{jets}) < 175^\circ$, $\Delta R(\text{jet} - \text{jet}) > 0.4$ and $p_T^{\text{miss}} > 40$ GeV. Normalisations are to unity at $\sqrt{s} = 14$ TeV (for $M_A = M_H = 300$ GeV in the case of the signal). Bins are 4 GeV wide.

$$\boxed{d^2\sigma/dR_1/dR_2/\sigma}$$

$b\bar{b}A \rightarrow \tau^+\tau^-X$ ($M_A = 300$ GeV)

$b\bar{b}H \rightarrow \tau^+\tau^-X$ ($M_H = 300$ GeV)



$t\bar{t} \rightarrow \tau^+\tau^-X$

$\gamma^*, Z \rightarrow \tau^+\tau^-X$

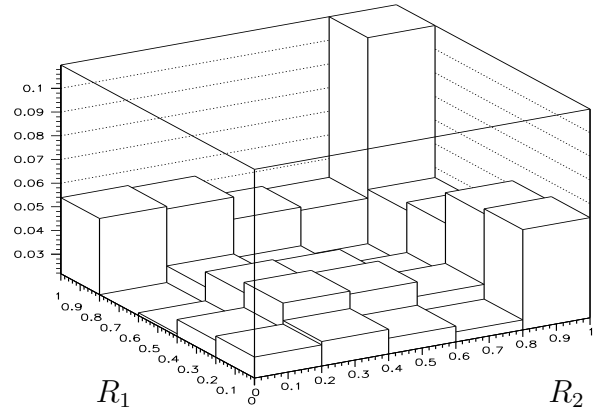
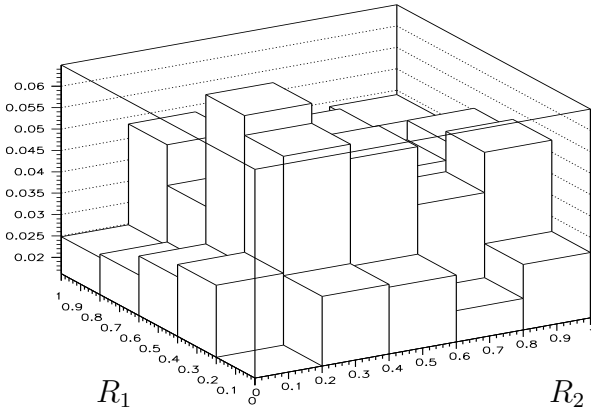


Figure 4: Doubly differential distributions in the energy fractions $R_i = p_i^{\pi^\pm}/p_i^{\tau\text{-jet}}$, where $p_i^{\pi^\pm}$ is the charged pion momentum and $p_i^{\tau\text{-jet}}$ that of the visible τ -jet, i.e, the momentum carried away by the mesons π^\pm, ρ^\pm and a_1^\pm in 1-prong decays, for Higgs signals and backgrounds in the $\tau^+\tau^-X$ channel (with $p_1 > p_2$), after the following selection cuts (at parton level): $p_T(\tau - \text{jet}_{1[2]}) > 100[60]$ GeV (1[2] refers to the most[least] energetic), $|\eta(\tau - \text{jet})| < 2.5$, $\Delta\Phi(\tau - \text{jets}) < 175^\circ$, $\Delta R(\text{jet-jet}) > 0.4$, $p_T^{\text{miss}} > 40$ GeV and $200 \text{ GeV} < M_{\tau\tau} < 400$ GeV. Normalisations are to unity at $\sqrt{s} = 14$ TeV (for $M_A = M_H = 300$ GeV in the case of the signal). Bins are 0.2 units wide.